ELSEVIER

Colloids and Surfaces
A: Physicochemical and Engineering Aspects 157 (1999) 223–233

COLLOIDS AND SURFACES A

www.elsevier.nl/locate/colsurfa

Thermocapillar instability of liquid sheets in motion☆

L.A. Dávalos-Orozco *

Instituto de Investigaciones en Materiales, Universidad Nacional Autónoma de México, Apartado Postal 70-360, Delegación, Coyoacán 04510, Mexico

Received 12 August 1998; accepted 24 February 1999

Abstract

In this paper the linear thermocapillar instability of a viscous liquid sheet in motion through a gas which has two free deformable surfaces with different temperatures is investigated. This temperatures difference is supposed to be due to a temperature gradient in the ambient gas. It is found that thermocapillar instability affects in an important way the viscosity-enhanced instability investigated by Li and Tankin (J. Fluid Mech. 226, (1991) 425). For the sinuous mode and small Weber numbers the viscosity destabilizes and thermocapillar effects destabilizes through the Marangoni number coupled to the Ohnesorge number, representing Viscous effects. The thermocapillar instability has growth rates far more larger than those of the pure viscosity-enhanced instability. For large Weber numbers Li and Tankin showed that the viscosity stabilizes and that the aerodynamic instability is the more important, however thermocapillarity destabilizes increasing the growth rates with the Ohnesorge number in such a way that for some Marangoni numbers the thermocapillar instability is the more important. Plots of the maximum growth rate against the Marangoni number are given in which new features of this maximum are observed such as a steep increase of its magnitude in a relatively small range of Marangoni numbers due to the onset of thermocapillary convection. It is shown that from the thermocapillar point of view the Weber number plays a stabilizing role. The varicose mode can not be changed notably by thermocapillarity and the curves almost remain the same as those of the pure viscosity-enhanced instability. For large enough values of the Marangoni and Ohnesorge numbers the sinuous mode has the larger maximum growth rate.

Keywords: Liquid sheet; Aerodynamic instability; Viscosity-enhanced instability; Thermocapillar instability; Marangoni instability

1. Introduction

The stability of liquid sheets in motion has recently attracted the attention of researchers due to its potential applications in, for example, swirl nozzles in gas burners where a hollow cone is formed by the thin liquid sheet. In general, the stability of liquid sheets is important in applications where the formation of drops is necessary to improve evaporation. This occurs after the break up of the liquid sheet due to non saturated growth of the perturbations.

The form of a non perturbed liquid sheet is shown in Fig. 1A and two modes of the perturba-

☆ This article was originally submitted to the 9th International Conference on Surface and Colloid Science

* Tel.: +52-5-6224601; fax: +52-5-6161201.

E-mail address: ldavalos@servidor.unam.mx (L.A. Dávalos-Orozco)

0927-7757/99/$ - see front matter
PII: S0927-7757(99)00093-X

tion are shown in Fig. 1B. The sinuous (or antisymmetric) mode corresponds to the two interfaces deforming in phase. The varicose (or symmetric) mode corresponds to the two surfaces deforming out phase by 180°.

Investigation of the stability of liquid sheets in motion were first made under the linear approximation of the equations of motion and supposing inviscid both the liquid sheet and the surrounding gas. In this case, only the velocity of the liquid and its interaction with that of the gas are the source of instability and the surface tension and density of the gas are stabilizing.

The stability of moving inviscid liquid sheets of uniform thickness was first investigated by Squire [1] and Hagerty and Shea [2]. Squire found that the sinuous disturbances are stable when the liquid Weber number is below the value $We = 1$.

This problem was extended by Dombrowski and Johns [3] to include the effects of viscosity but with an additional approximation of large Weber numbers. The complete stability calculation of the viscous sheet in motion, valid for any Weber numbers, was first done by Li and Tankin [4]. They obtained very interesting results concerning also to the inviscid liquid sheet. They show that the inviscid liquid sheet is more unstable for the varicose mode for small Weber numbers. Furthermore, after certain value of the Weber number the sinuous mode is the more unstable. Including viscosity by means of the Ohnesorge number Z two kinds of instabilities appear, they are the aerodynamic, due to the velocity difference between the liquid and the gas, and the viscosity-enhanced, due to viscosity. For the sinuous mode when We is small, but above the critical, the viscosity-enhanced instability has a larger maximum growth rate than the aerodynamic instability for large values of Z. When We is large the aerodynamic instability is more important and viscosity stabilizes when Z increases and, at the same time, the wavenumber corresponding to the maximum growth rate decreases. For the varicose mode they found that the aerodynamic instability is always the more unstable and that viscosity is stabilizing for all Weber numbers.

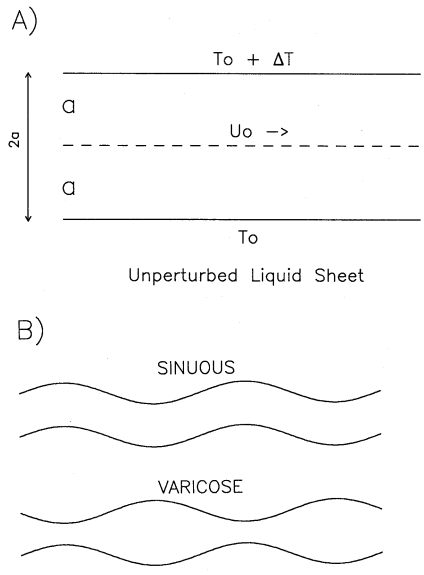

Fig. 1. (A) The unperturbed liquid sheet of thickness $2a$ in motion with velocity U_o and a difference in temperatures between the upper and lower free surfaces. (B) Two modes of instability possible in the perturbed liquid sheet, the sinuous (or antisymmetric) mode and the varicose (or symmetric) mode.

In this paper, the linear thermocapillar instability of a liquid sheet in motion which is supposed to be in the presence of a temperature gradient perpendicular to the sheet is investigated. This condition may arise inside the gas in burners of gas-turbine combustors where no control of the uniformity of temperature exist. Buoyancy effects are ignored in the sheet and the gas.

Investigation of thermocapillar instability of static liquid sheets with two deformable free surfaces has been done by Funada [5] and Oron et al. [6]. Funada [5] calculated the lines of criticality for non deformable and deformable free surfaces. Besides, he investigated the effect of the deviation of surface tension from its mean value due to a temperature gradient and the effects of Biot number. Oron et al. [6] investigated, for zero Biot number, the instability of the sinuous mode when the Marangoni and crispation numbers are different at the cold and hot surfaces. They obtain criticality curves for the stationary

and time dependent instabilities and their relation with the Prandtl number.

In this paper a combination of both phenomena, thermocapillarity and the motion of the liquid sheet interacting with the gas will be investigated. The number of parameters is too large and therefore calculations will be restricted to special cases. Thus, the Biot number is supposed zero (the more unstable situation) and the Prandtl number is set to that of water, that is, $\mathrm{Pr} = 7$. Besides. as shown later, it is found that the Crispation number is related to the Ohnesorge and the Prandtl numbers. The gas–liquid density ratio is fixed at $\rho = 0.1$ in order to compare results with those of Li and Tankin [4]. To the author knowledge this problem has not been investigated and is a first step to a more general situation in which ρ, the Biot and Prandtl numbers are arbitrary. Calculations of the more general case are in progress.

Here, we must point out that the problems investigated in papers [5] and [6] are not completely related to the present one when the velocity of the liquid sheet is made zero ($\mathrm{We} = 0$). The reason is that in those papers they are ignoring the perturbation of the gas velocity which is transmitted to the liquid sheet through the gas pressure and do not take into account the gas–liquid densities ratio ρ. Therefore, we are doing calculations for the thermocapillary convection of the static liquid sheet under this new conditions. In this paper, results will be restricted to the parameters already selected.

The important effect of evaporation (see for example Refs. [7] and [8]) at the free surfaces is not included in our calculations. One reason is that the main interest of this paper is to investigate the purely thermocapillary effects in comparison which viscous instabilities. Besides, the number of parameters involved is so large that some of them will already be fixed in this paper.

The structure of the paper is as follows. In Section 2 the equations of motion of the one component pure liquid sheet and the gas are presented and the dispersion relation is obtained. In Section 3 we give the results of the numerical analysis of the dispersion relations. Section 4 corresponds to the discussion and conclusions.

2. Equations of motion and dispersion relations

The equations of motion and energy are given for a one component pure liquid sheet in motion in the x-direction with velocity U_o. The origin of the coordinate system is supposed at the middle of the sheet and the two non perturbed free surfaces are set at $y = \pm a$, therefore the thickness of the liquid sheet is $2a$. One free surface has temperature T_o and the other one has temperature $T_o + \Delta T$, as shown in Fig. 1A. This generates a temperature gradient across the sheet which produces heat transfer from the hotter to the colder one, changing at the same time the magnitude of the corresponding surface tensions. The changes in surface tensions produces surface shear influencing the stability of the liquid sheet which may be already stable or unstable independently of the temperature gradient [4], due to aerodynamic or viscosity-enhanced instability.

The liquid sheet has density ρ_l, kinematic viscosity ν_l, thermal diffusivity κ and satisfies the two dimensional system of mass, momentum and energy balance equations:

$$\frac{\partial u}{\partial t} + U_o\frac{\partial u}{\partial x} = -\frac{1}{\rho_l}\frac{\partial p}{\partial x} + \nu_l\nabla^2 u \tag{1}$$

$$\frac{\partial u}{\partial t} + U_o\frac{\partial v}{\partial x} = -\frac{1}{\rho_l}\frac{\partial p}{\partial y} + \nu_l\nabla^2 v \tag{2}$$

$$\frac{\partial T}{\partial t} + U_o\frac{\partial T}{\partial x} = \kappa\nabla^2 T \tag{3}$$

$$\frac{\partial u}{\partial x} + \frac{\partial v}{\partial y} = 0 \tag{4}$$

where the Laplacian is defined as:

$$\nabla^2 = \frac{\partial^2}{\partial x^2} + \frac{\partial^2}{\partial y^2} \tag{5}$$

The velocity components of the viscous liquid are separated into:

$$u = u_1 + u_2$$

$$v = v_1 + v_2 \tag{6}$$

Following Li and Tankin (1991) the pair (u_1, u_2) represents an inviscid irrotational flow and the pair (v_1, v_2) has the viscous effects, including the

thermocapillar ones. Here, p is the pressure and T is the temperature of the viscous liquid.

The gas of density ρ_g is inviscid and satisfies the Euler equations:

$$\frac{\partial u_g}{\partial t} = -\frac{1}{\rho_g}\frac{\partial p_g}{\partial x} \tag{7}$$

$$\frac{\partial v_g}{\partial t} = -\frac{1}{\rho_g}\frac{\partial p_g}{\partial y} \tag{8}$$

$$\frac{\partial u_g}{\partial x} + \frac{\partial v_g}{\partial y} = 0 \tag{9}$$

The liquid and the gas are coupled by the boundary conditions at $y = \pm a$. They are: Stresses balance at $y = \pm a$:

$$(\sigma_{l,\,ij} - \sigma_{g,\,ij})n_j = \sigma\kappa_c(\eta)n_i - \gamma t_i\left(t_j\frac{\partial T}{\partial x_j}\right) \tag{10}$$

Fixed heat flux H at $y = \pm a$:

$$H = const. \tag{11}$$

Kinematic boundary condition at $y = \pm a$:

$$\frac{\partial \eta}{\partial t} + U_o\frac{\partial \eta}{\partial x} = v_l \tag{12}$$

and for the gas velocity:

$$\frac{\partial \eta}{\partial t} = v_g \tag{13}$$

The gas velocity at $y = \pm \infty$:

$$v_g = 0 \tag{14}$$

where $\sigma_{l,\,ij}$ is the stress tensor, $\sigma_{g,\,ij}$ only represents the gas pressure, σ is the surface tension, $\kappa_c(\eta)$ is the surface curvature, η is the surface deformation and

$$\gamma = -\frac{\partial \sigma}{\partial T}.$$

The vector n_j is the normal vector to the surface and t_j is its tangent vector. H is the heat passing through the liquid sheet which here will be considered fixed. (In this case the Biot number will be zero).

The variables are made non dimensional as follows. Lengths are scaled with a. time with $(\rho_l a^3/\sigma)^{1/2}$, velocity with $(\sigma/\rho_l a)^{1/2}$, pressure with σ/a and temperature with $\beta a = \Delta T$.

The temperature profile of the main flow is

$$T_m = \frac{\Delta T}{2}\left(\frac{y}{a} + 1\right) + T_0$$

where T_m is the temperature in dimensional form. A perturbation of the non dimensional variables in normal modes of the form $f(x, t) = F(y)\exp(\omega + imx)$ is used. Here, $\omega = \omega_r + i\omega_i We^{1/2}$ and m is the wavenumber. ω_r and ω_i are, respectively, the growth rate and wave velocity of the perturbation. $We = \rho_l U_o^2 a/\sigma$ is the Weber number of the liquid which represents the ratio of inertial to capillary forces. The equations of motion, heat diffusion and boundary conditions become:

$$D^2\Phi - m^2\Phi = 0 \tag{15}$$

$$D^2\Psi - s^2\Psi = 0 \tag{16}$$

$$D^2\Theta - r^2\Theta = \frac{Pr}{Z}(D\Phi - im\Psi) \tag{17}$$

$$D^2\Phi_g - m^2\Phi_g = 0 \tag{18}$$

The kinematic boundary condition:

$$D\Phi - im\Psi = (\omega + im We^{1/2})\xi_0 \qquad \text{at } y = \pm 1 \tag{19}$$

The normal stresses:

$$2Z(D^2\Phi - imD\Psi) = P - m^2\xi_0 - \rho\omega\xi_0/m \quad \text{at } y = 1 \tag{20}$$

$$2Z(D^2\Phi - imD\Psi) = P - m^2\xi_0 - \rho\omega\xi_0 e^{i\theta}/m \qquad \text{at } y = -1 \tag{21}$$

The tangential stresses:

$$-2m^2D\Phi + im(D^2\Psi + m^2\Psi) = m^2ZM(\Theta + \xi_0)/Pr \qquad \text{at } y = 1 \tag{22}$$

$$-2m^2D\Phi + im(D^2\Psi + m^2\Psi) = m^2ZM(\Theta + \xi_0 e^{i\theta})/Pr \qquad \text{at } y = -1 \tag{23}$$

The heat flux is fixed at the free surfaces:

$$D\Theta = 0 \qquad \text{at } y = \pm 1 \tag{24}$$

The boundary conditions for the gas are:

$$D\Phi_g = \omega\xi_0 \qquad \text{at } y = \pm 1 \tag{25}$$

$$D\Phi_g = 0 \qquad \text{at } y = \pm \infty \tag{26}$$

$$T_{gyy} = -P_g = \rho\frac{\partial \Phi_g}{\partial t} \qquad \text{at } y = \pm 1 \tag{27}$$

where $s^2 = m^2 + (\omega + im\mathrm{We}^{1/2})/Z$ and $r^2 = m^2 + \mathrm{Pr}(\omega + im\mathrm{We}^{1/2})/Z$ and Φ, Φg, Ψ, Θ, ξ_0, P and P_g are the amplitudes of the velocity potential, the gas velocity potential, the current function, the temperature, the surfaces deformation, liquid pressure and the gas pressure, respectively. T_{gyy} represents the gas normal stresses. The parameter θ is the phase difference between the upper free surface and the lower free surface deformation. Here, it will be $\theta = 0$ (sinuous case) or π (varicose case).The following non dimensional parameters has also been used. $Z = v_l(\rho_l/\sigma a)^{1/2}$ is the Ohnesorge number (representing the ratio of viscous to capillary forces), $\rho = \rho_g/\rho_l$ is the gas-liquid density ratio, $\mathrm{Pr} = v_l/\kappa$ is the Prandtl number, $\mathrm{Ma} = \gamma\beta a^2/\rho_l v_l \kappa$ is the Marangoni number (which represents the ratio of thermocapillary to viscous forces) and

$$\beta = \frac{\Delta T}{2a}.$$

It was found that the Crispation number satisfies the following relation $\mathrm{Cr} = \mathrm{Z}^2/\mathrm{Pr}$.

Applying to the boundary conditions the solutions of the system of equations for the perturbations and following the same procedure as Li and Tankin [4], a set of six homogeneous equations with six unknowns is obtained (in [4] they were 4). As solution of this set the following eigenvalue equations are obtained:

Sinuous case:

$$\frac{1}{G_1}[Q_1 \tanh m\{(Br \tanh r - CsE \tanh s)X_1 + Cmr \tanh r\} - Q_2 \tanh s\{(Ar \tanh r - CDm \tanh m)X_1 + Cmr \tanh r\} + Q_3 = 0 \quad (28)$$

Varicose case:

$$\frac{1}{G_2}[Q_1\{-(iCEs \tanh r - Br \tanh s)X_1 + Cmr \tanh s\} - Q_2\{(CDm \tanh r + Ar \tanh m)X_1 + Cmr \tanh r\} + Q_3 = 0 \quad (29)$$

where the following symbology has been used including non dimensional parameters:

$$G_1 = m\{C(Dm \tanh m - Es \tanh s) + r(B - A) \tanh r\} \quad (30)$$

$$G_2 = m\{r(B - A) \tanh m \tanh s - C \tanh r(iEs \tanh m + Dm \tanh s)\} \quad (31)$$

$$Q_1 = 2Zm^2 + (\omega + im\mathrm{We}^{1/2}) \quad (32)$$

$$Q_2 = 2\mathrm{Z}ms \quad (33)$$

$$Q_3 = m^2 + \frac{\omega^2}{m}\rho \quad (34)$$

$$X_1 = \omega + im\mathrm{We}^{1/2} \quad (35)$$

$$A = m^3\left[2 + \frac{\mathrm{Ma}}{m^2 - r^2}\right] \quad (36)$$

$$B = m\left[s^2 + m^2 + \frac{m^2\mathrm{Ma}}{s^2 - r^2}\right] \quad (37)$$

$$C = \frac{m^2 Z\mathrm{Ma}}{\mathrm{Pr}} \quad (38)$$

$$D = \frac{\mathrm{Pr}m}{Z(m^2 - r^2)} \quad (39)$$

$$E = \frac{\mathrm{Pr}m}{Z(s^2 - r^2)} \quad (40)$$

3. Results of numerical analysis

The dispersion relations Eq. (12) and Eq. (13) are solved by the Muller method. The results of numerical analysis will be done using the same values of the parameters used by Li and Tankin [4] in order to make a comparison easy to understand. Except that, instead of $Z = 0.1$, use is made of $Z = 1$. For the thermal problem the Biot number is set equal to zero and the Prandtl number is $\mathrm{Pr} = 7$ corresponding to that of water. Instead of the Weber number for the gas (used in [4]) use is made of We, the Weber number of the liquid. The gas Weber number is simply given by the product $\rho\mathrm{We}$. Note that for the sake of comparison, the gas–liquid density ratio is also supposed $\rho = 0.1$, as Li and Tankin [4], even though it is larger than that of most practical systems.

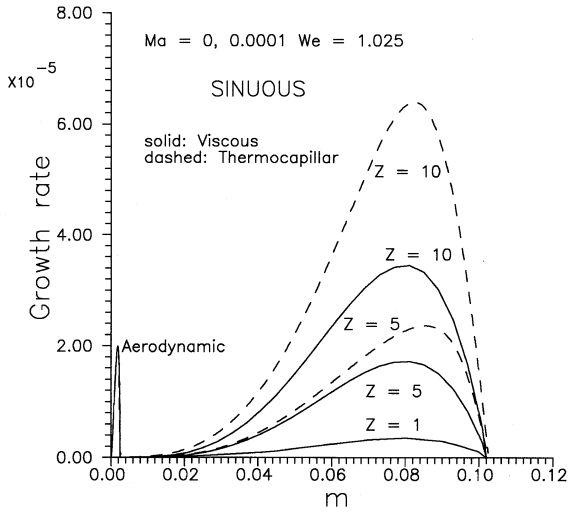

Fig. 2. Sinuous mode. Growth rate against wavenumber with $Ma = 0.0001$ and $We = 1.025$. Comparison of the viscosity-enhanced instability (solid) curves with the thermocapillar instability (dashed) curves and the aerodynamic instability curve (left hand side). The maximum growth rate increases considerably for a very small Ma. Note the scales in the vertical axis.

In Fig. 2 results of the thermocapillary instability of the sinuous mode are presented when $We = 1.025$, just above the critical value for instability in the inviscid liquid [1]. The interpretation is that the velocity is relatively small even though the sheet is already unstable. This figure presents plots of the growth rate against the wavenumber m. To the left, it is found the aerodynamic stability curve. To the right, the solid lines correspond to the viscosity-enhanced instability. The dashed lines correspond to thermocapillarity coupled to the viscosity-enhanced instability. It is clear that even a very small Marangoni number allows viscosity to destabilize by means of the Ohnesorge number to almost twice the magnitude of the growth rate corresponding to that of the simple viscosity-enhanced instability, when $Z = 10$. In this case a small Ma can not excite the small viscous effect of $Z = 1$. Here an increase of the Ohnesorge number means that the viscous forces become relatively more important than the capillary forces. Therefore, the viscosity has a destabilizing effect which is enhanced by thermocapillarity.

In Fig. 3 it is shown how the interaction of viscous and thermocapillar effects can be very effective at the same value of We. Note the scales in each figure. In Fig. 3a it is shown that the growth rate of the viscous curve (solid) for $Z = 1$

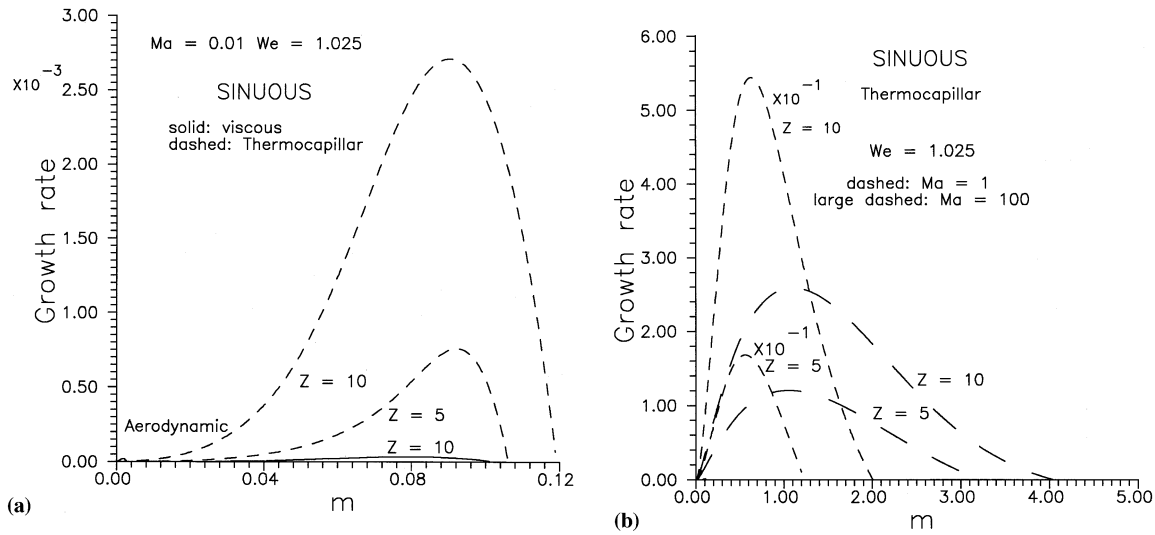

Fig. 3. Sinuous mode. Growth rate against wavenumber with $We = 1.025$. Comparison of the viscosity-enhanced instability (solid) curves with the thermocapillar instability (dashed) curves and the aerodynamic instability curve (left hand side). Note the scale in each figure. (a) For $Ma = 0.01$. The viscosity-enhanced instability (solid) curve for $Z = 10$ and the aerodynamic instability curve (left hand side) are almost imperceptible. (b) $Ma = 1$ (note scale $\times 10^{-1}$ in dashed curves) and $Ma = 100$ (large dashed curves).

is already invisible and that the curve for $Z = 10$ is almost imperceptible. Besides, it is shown that the corresponding curve of aerodynamic instability is visible only as a small spike. A change in two orders of magnitude in Ma changes two orders of magnitude the growth rate of $Z = 5$ and $Z = 10$, as observed in Fig. 2 and Fig. 3a. However, this does not occur for the change from $\mathrm{Ma} = 1$ to $\mathrm{Ma} = 100$ where only an increase of one order of magnitude is observed in the growth rate as shown in Fig. 3b. Here, the increase in temperature gradient and its interaction with viscous effects is not as effective as for small gradients. This will be discussed later from a different stand point in a plot of the maximum growth rate against Ma. Note in Fig. 3b that the magnitude of the growth rate of the dashed curves must be multiplied by 10^{-1} to have the correct value.

In the isothermal case, when the velocity increases to give a large We the viscosity stabilizes through Z, as shown in [4]. However, as shown here for $\mathrm{We} = 40$, thermocapillarity allows viscosity to destabilize in the same way as for small We. These results are presented in Fig. 4 where it is shown that the aerodynamic instability is the more unstable for isothermal conditions or for small Ma. Fig. 4a shows that $\mathrm{Ma} = 1$ is not enough to make a great difference in the stability but note that it already changed the order in which the growth rate increases with Z in comparison with the isothermal case (solid lines). This change in the order of the curves with respect to Z shows that thermocapillar effects do not allow the viscous ones to stabilize while they are interacting. Hence, here a more viscous liquid sheet (larger Z) is more unstable. Moreover, Fig. 4b for $\mathrm{Ma} = 40$ shows that the interaction with thermocapillarity allows viscosity to reach the maximum of the aerodynamic instability curve for $Z = 10$. In Fig. 4c for $\mathrm{Ma} = 80$ it is possible to surpass notably the maximum of the aerodynamic instability curve. Therefore, if the fluid is relatively highly viscous and the temperature gradient is large enough, the coupling of thermocapillar and viscous effects will be more relevant than inviscid aerodynamic instabilities for large We.

Here, it should be noted that the increase in We made it necessary to increase Ma considerably to let thermocapillary instability interact with viscosity effectively. Notice that the curve for $\mathrm{Ma} = 80$ and $Z = 10$ in Fig. 4c attains almost the same maximum as the corresponding large dashed curve of Fig. 3b. This means that for small and large velocities almost the same high temperature gradient is required to attain these large growth rates. This will be discussed further presently.

For the varicose mode only some results are presented. The reason is that, as observed in Fig. 5, even for very large values of Ma the curves of thermocapillarity do not invert in the order of magnitude of Z as in the sinuous case. There is almost no difference between curves for $\mathrm{Ma} = 100$ and $\mathrm{Ma} = 1000$, for example. Moreover, there is almost no difference between the viscosity-enhanced and thermocapillarity curves for any value of Ma. However, it was possible to increase the growth rate of the thermocapillary curve decreasing Z until the thermocapillary curve merged with the aerodynamic one (non viscous effects). In spite of all these properties of the varicose mode we have shown in Fig. 4c that the aerodynamic instability of the sinuous mode is more unstable than this one and, moreover, that the thermocapillary instability is the most unstable if $\mathrm{Ma} > 40$ for $Z = 10$ when both $\mathrm{We} = 1.025$ and 40 (Fig. 3b and Fig. 4c).

The wave velocity, made non dimensional with the liquid sheet velocity U_o, has interesting characteristics for different values of Ma. Graphs of the wave velocity against the wavenumber are shown in Fig. 6. For $\mathrm{We} = 1.025$ and $\mathrm{Ma} = 10^{-4}$ and $\mathrm{Ma} = 10^{-2}$, Fig. 6 shows that the wave velocities have no difference with the thermocapillary case for $Z = 1, 5, 10$ (large dashed curve). The aerodynamic wave velocity has not been included because, as it is easily seen in Fig. 3a, its wave number range is confined to values very near to zero in comparison with those of thermocapillary instability. For $\mathrm{Ma} = 1$, Fig. 6 shows the wave velocities for two values of $Z = 1, 10$ (large dashed and stared curves, respectively). Notice that there is no difference with respect to the thermocapillary ones. The more viscous the liquid is the more smoothly it tends to the maximum of one. Therefore, the dimensional phase velocity is always smaller than the liquid sheet velocity and

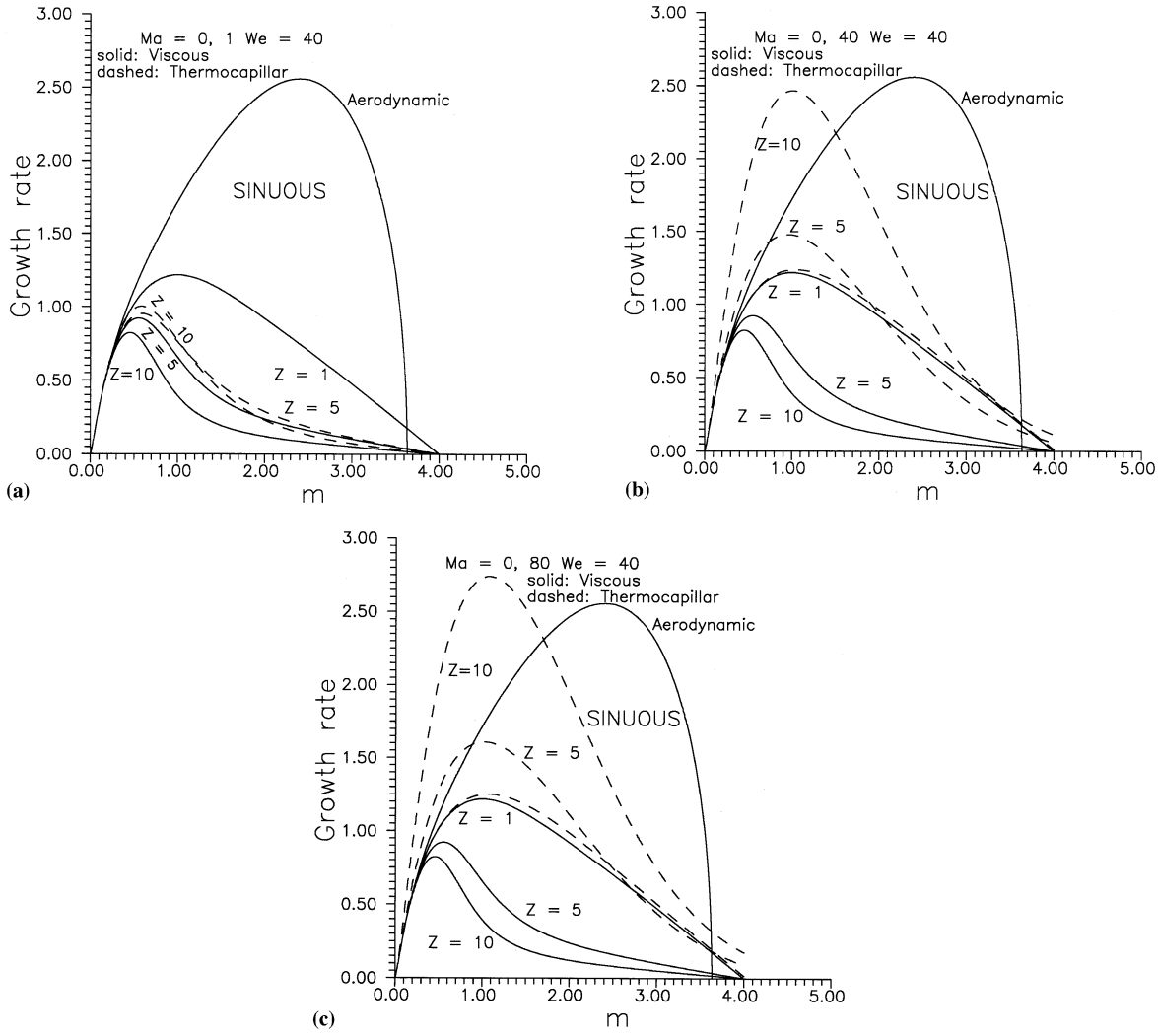

Fig. 4. Sinuous mode. Growth rate against wavenumber with We = 40 for different values of Z. Comparison of the viscosity-enhanced instability (solid) curves with the thermocapillar instability (dashed) curves and the aerodynamic instability curve. Viscosity destabilizes due to thermocapillar instability, contrary to the results found for the viscosity-enhanced instability [4]. (a) Ma = 1. (b) Ma = 40. The thermocapillar instability almost reaches the maximum growth rate of the aerodynamic instability which is surpassed when (c) Ma = 80.

tends to the later for large wavenumbers. It tends to zero to very small wavenumbers. When We = 40 and Ma = 80, Fig. 6 shows that, except for $Z = 1$, a difference exists between the wave velocities of the viscosity-enhanced and the thermocapillary instabilities (the thermocapillar dashed curves are almost superposed for $Z = 5$ and 10).

A more detailed understanding of the results presented in this paper may be obtained by means of graphs of the maximum growth rate and its corresponding wavenumber against the Marangoni number. Thus, Fig. 7 shows results for the sinuous mode when We = 1.025 and 40. A log-log plot of the maximum growth rate against Ma is presented. Here for We = 1.025 (solid curves), it is seen how the maximum growth rate increases with Z and Ma. Note also that for the values of Z, except $Z = 1$, there is a Ma range at

which an abrupt increase occurs. After this range a plateau is reached from which the maximum growth has almost no increase with Ma. It is difficult to see but the curve for $Z=1$ has a maximum near to log(Ma) = 2.2. Related with this abrupt increase in curves $Z=5, 10$ is an abrupt increase of the corresponding wave number in the same range of Ma, as shown in Fig. 8 for We = 1.025. It is interesting to observe in this figure that the wavenumber also reaches a plateau at which it increases very slowly with Ma. However, for $Z=1$, the wavenumber does not tend to a constant value but instead it decreases with Ma after attaining a maximum. Notice how the curves cross to each other at some values of Ma.

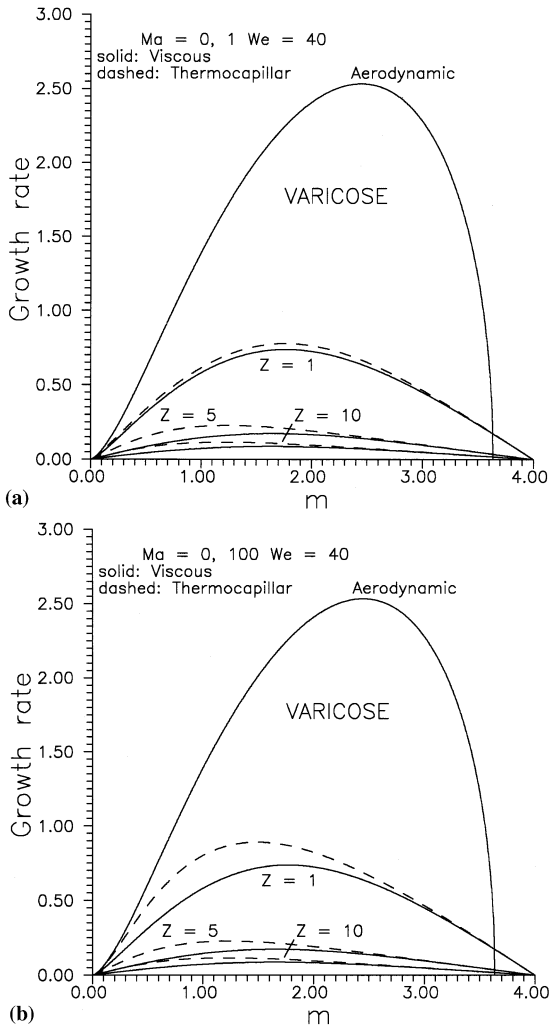

Fig. 5. Varicose mode. Growth rate against wavenumber with We = 40 for different values of Z. Comparison of the viscosity-enhanced instability (solid) curves with the thermocapillar instability (dashed) curves and the aerodynamic instability curve. (a) Ma = 1, (b) Ma = 100. There is almost no change in the curves with these relatively large Marangoni numbers.

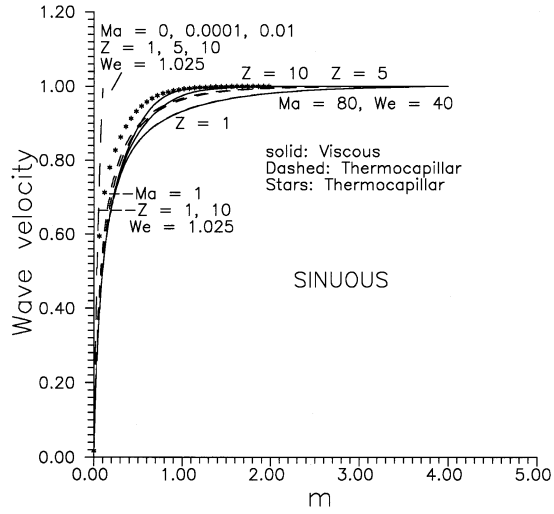

Fig. 6. Sinuous mode. Wave velocities against wavenumber with We = 1.025 and different values of Z. The large dashed curve is for We = 1.025 and Ma = 0, 10^{-4}, 10^{-2} where the thermocapillar and viscous curves are superposed. The large dashed curve ($Z=1$) and the starred curve ($Z=10$) are for We = 1.025 and Ma = 1 where also the thermocapillar and viscous curves are superposed. For We = 40 and Ma = 80 the dashed curves are thermocapillar and solid curves are viscous.

For the sinuous mode and We = 40, Fig. 7 shows plots (dashed curves) similar to those of We = 1.025 for three values of Z. Observe the small difference in the growth rates. In the figure the curves cross each other at different values of Ma. In this case, there is also a range of Ma at which an abrupt increase in the maximum growth rate occurs, in the same order of Z as in We = 1.025, exception made for $Z=1$. Note also that, for the tendency of the curves, a crossing between them must also occur for We = 1.025, but for a much smaller value of Ma. Fig. 8 shows the corresponding wavenumbers (dashed curves for We = 40) which cross to each other for a larger magnitude of Ma and which also have an abrupt increase in magnitude in the same range as for the maximum growth rate.

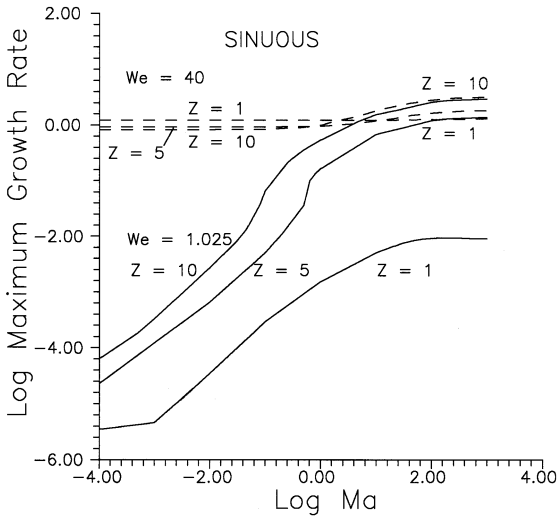

Fig. 7. Sinuous mode. Log–log plots of the maximum growth rate against Ma. The continuous curves are for We = 1.025 and different values of Z. The dashed curves are for We = 40 and different values of Z.

The abrupt increase of the maximum growth rate is explained by thermocapillary convection. Numerical analysis for We = 0 (zero velocity) shows that $Z = 1$ is always thermocapillary stable from $Ma = 10^{-4}$ to 10^{6} (for the parameters used in this paper). Results for $Z = 5$ show that thermocapillarity starts at $Ma_c = 0.465$ and $m_c = 0.658$, which corresponds to the Ma at which the abrupt increase occurs, see Fig. 7 when the influence of We is not strong. Thus, the magnitude of m_c is that at which the liquid sheet tries to adjust after thermocapillary convection occurs. However, the critical wavenumber m_c is larger than the plotted one meaning that a small liquid sheet velocity, through We, is able to decrease the wavenumber corresponding to the maximum growth rate. The critical values for $Z = 10$ are $Ma_c = 0.0973$ and $m_c = 0.564$.

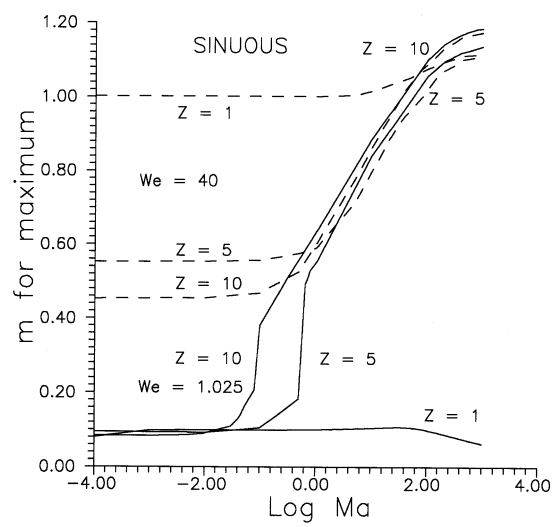

Fig. 8. Sinuous mode. Graphs of the wavenumber against the logarithm of Ma. The continuous curves are for We = 1.025 and different values of Z. The dashed curves are for We = 40 and different values of Z.

After the abrupt jump thermocapillarity (Ma) and viscosity (Z) work together to change the slope of the curves of maximum growth. This is also seen in Fig. 8 for the corresponding wavenumber. However, large sheet velocities not only delays thermocapillary instability to a larger Ma_c (larger temperature gradients) but also make it have smaller slops in the graphs of maximum growth rate against Ma as shown in Fig. 7. From this point of view, the We has stabilizing effects on the liquid sheet.

For the We, Z and Ma used in Fig. 7 and Fig. 8, it was possible to obtain growth rates larger than those of the aerodynamic instability. Therefore, when We is large it is not possible for Ma or Z alone to increase the growth rates. It is necessary to increase both to a large enough magnitude. For example, for We = 100 it is necessary to have $Z = 40$ and Ma = 100 to let thermocapillarity be the most unstable. There is almost no change if, at $Z = 40$, Ma is increased alone to, lets say, 1000.

From a comparison of Fig. 2 and Fig. 3 with Fig. 4 and of the results of Fig. 7 for We = 1.025 and 40, we may say that an increase in Weber number (or sheet velocity) smoothes out the important changes thermocapillary instability may produce on the liquid sheet.

4. Conclusions

From the results presented above the following important conclusions are drawn.

For the isothermal sheet the aerodynamic varicose mode is the most unstable for small Weber numbers, but we have shown that thermocapillar effects in the sinuous mode may be more important than the aerodynamic and viscous instabilities in both the sinuous and varicose modes. Increasing We in the varicose mode, the aerodynamic instability remains as the more unstable even in the presence of thermocapillarity. In this mode thermocapillarity does not change considerably the magnitude of the growth rate and the curves are qualitatively the same as those of reference [4]. However, when $We = 40$ and $Ma > 40$ the thermocapillary sinuous mode is more unstable than the aerodynamic and viscosity enhanced varicose and sinuous modes. Therefore, it is believed that the sinuous mode has more possibilities to appear than the varicose mode under large enough Ma and Z, even when the Weber number is large.

For the sinuous mode, thermocapillar effects produce a fast increase of both the maximum growth rate and the corresponding wavenumber in certain small range of values of the Marangoni number. It is shown that the fast increase is due to the onset of thermocapillary convection in the liquid sheet and that it is delayed to larger Ma_c by an increase of Weber number. In this sense, the liquid sheet velocity, through We, plays a stabilizing role. The magnitude of Ma necessary for its occurrence is smaller when Z decreases, that is, for smaller viscous effects.

A possible experimental set up to check our results could be a chamber, containing a gas like air, with a heated upper wall and a cooled lower wall which will set a stabilizing temperature gradient in order to avoid buoyancy effects in the gas. A thin liquid sheet, ejected horizontally across the chamber. will feel the temperature gradient and show thermocapillar instability, destabilizing in a different way in comparison to the isothermal viscosity enhanced case.

Acknowledgements

The author would like to thank DGAPA-UNAM for support to project IN106797. Besides, thanks are due to Mr. Paul Reyes for technical support.

References

[1] H.B. Squire, Br. J. Appl. Phys. 4 (1953) 167.
[2] W.W. Hagerty, J.F. Shea, J. Appl. Mech. 22 (1955) 509.
[3] N. Dombrowski, W.R. Johns, Chem. Eng. Sci. 18 (1963) 203.
[4] X. Li, R.S. Tankin, J. Fluid Mech. 226 (1991) 425.
[5] T. Funada, J. Phys. Soc. Jpn. 55 (1986) 2191.
[6] A. Oron, R.T. Deissler, J.C. Duh, Adv. Space Res. 16 (7) (1995) 83.
[7] J.P. Burelbach, S.G. Bankoff, S.H. Davis, J. Fluid Mech. 195 (1988) 463.
[8] S.W. Joo, S.H. Davis, S.G. Bankoff, J. Fluid Mech. 230 (1991) 117.